Molecular Cell

Article

Single-Cell Tracing Dissects Regulation of Maintenance and Inheritance of Transcriptional Reinduction Memory

Graphical Abstract

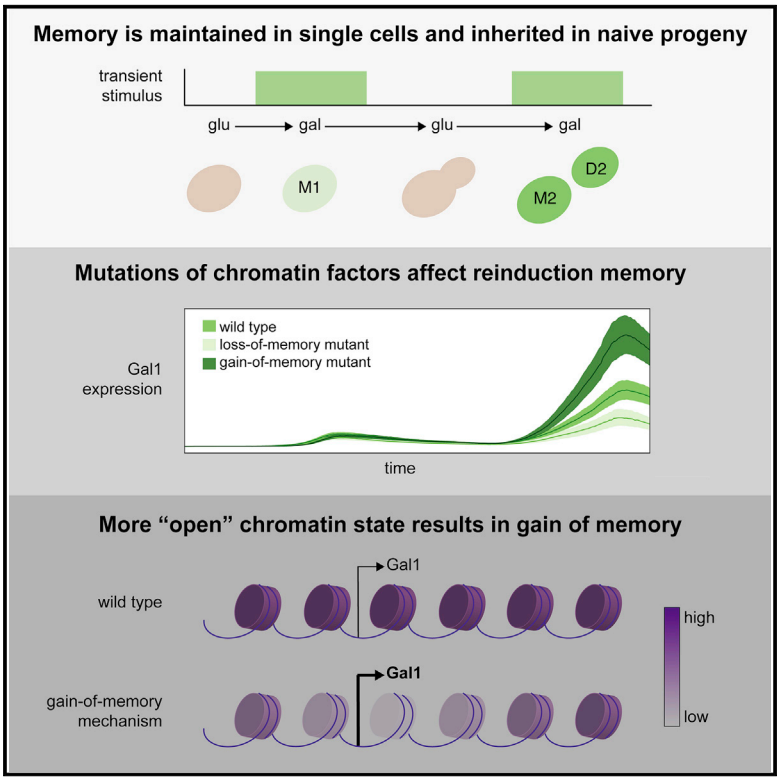

Highlights

- Single yeast cells maintain memory of gene induction and transmit it to naive progeny
- Pedigree analysis shows memory capacity is similar within lineages
- Screens reveal chromatin factors involved in memory maintenance and/or inheritance
- A memory mutant is identified with enhanced reinduction memory

Authors

Poonam Bheda, Diana Aguilar-Gómez, Nils B. Becker, ..., Carsten Marr, Antonis Kirmizis, Robert Schneider

Correspondence

kirmizis@ucy.ac.cy (A.K.), robert.schneider@helmholtz-muenchen.de (R.S.)

In Brief

Bheda et al. adopt single-cell approaches to show that Gal1 transcriptional memory in yeast is maintained in mothers and inherited by daughters in the absence of the galactose stimulus. Subsequent high-throughput systematic screens identify chromatin factors implicated in these processes and unveil a gain-of-memory phenotype.

Bheda et al., 2020, Molecular Cell *78*, 915–925
June 4, 2020
https://doi.org/10.1016/j.molcel.2020.04.016

CellPress

Molecular Cell

CellPress

Article

Single-Cell Tracing Dissects Regulation of Maintenance and Inheritance of Transcriptional Reinduction Memory

Poonam Bheda,[1] Diana Aguilar-Gómez,[1,2,3] Nils B. Becker,[4,11] Johannes Becker,[5,11] Emmanouil Stavrou,[6] Igor Kukhtevich,[1] Thomas Höfer,[4] Sebastian Maerkl,[5] Gilles Charvin,[7] Carsten Marr,[8] Antonis Kirmizis,[6,*] and Robert Schneider[1,9,10,12,*]

[1]Institute of Functional Epigenetics, Helmholtz Zentrum München, 85764 Neuherberg, Germany
[2]Center for Genomic Sciences, UNAM, 62210 Cuernavaca, Mexico
[3]Center for Computational Biology, University of California, Berkeley, Berkeley, CA 94720, USA
[4]Theoretical Systems Biology, DKFZ, 69120 Heidelberg, Germany
[5]Institute of Bioengineering, School of Engineering, École Polytechnique Fédérale de Lausanne, 1015 Lausanne, Switzerland
[6]Biological Sciences, University of Cyprus, 2109 Nicosia, Cyprus
[7]Development and Stem Cells, IGBMC, 67400 Illkirch, France
[8]Institute of Computational Biology, Helmholtz Zentrum München, 85764 Neuherberg, Germany
[9]German Center for Diabetes Research (DZD), 85764 Neuherberg, Germany
[10]Faculty of Biology, Ludwig-Maximilians Universität München, Munich, Germany
[11]These authors contributed equally
[12]Lead Contact
*Correspondence: kirmizis@ucy.ac.cy (A.K.), robert.schneider@helmholtz-muenchen.de (R.S.)
https://doi.org/10.1016/j.molcel.2020.04.016

SUMMARY

Transcriptional memory of gene expression enables adaptation to repeated stimuli across many organisms. However, the regulation and heritability of transcriptional memory in single cells and through divisions remains poorly understood. Here, we combined microfluidics with single-cell live imaging to monitor *Saccharomyces cerevisiae* galactokinase 1 (*GAL1*) expression over multiple generations. By applying pedigree analysis, we dissected and quantified the maintenance and inheritance of transcriptional reinduction memory in individual cells through multiple divisions. We systematically screened for loss- and gain-of-memory knockouts to identify memory regulators in thousands of single cells. We identified new loss-of-memory mutants, which affect memory inheritance into progeny. We also unveiled a gain-of-memory mutant, *elp6Δ*, and suggest that this new phenotype can be mediated through decreased histone occupancy at the *GAL1* promoter. Our work uncovers principles of maintenance and inheritance of gene expression states and their regulators at the single-cell level.

INTRODUCTION

When certain genes are repeatedly exposed to the same stimulus, they can adapt subsequent responses. This so-called transcriptional reinduction memory is important for the adaptation of gene expression across various organisms. Emerging evidence suggests that transcriptional memory could have important consequences on cell survival and identity (Foster et al., 2007; Francis and Kingston, 2001), and that it could have implications for disease progression (e.g., in diabetes) (Villeneuve et al., 2011) and innate immunity in humans (Foster et al., 2007). Thus, a comprehensive understanding of transcriptional memory has become increasingly important.

Although an epigenetic basis for some reinduction memory systems has been suggested (Avramova, 2015; Berry et al., 2017; D'Urso and Brickner, 2017; Iberg-Badeaux et al., 2017), there has been a lack of approaches and measures to quantify the maintenance and inheritance of memory through cell divisions, mainly due to the use of bulk cell populations, which masks single-cell behavior. To address the potential epigenetic nature of such a transcriptional memory, tracking of single cells over multiple cellular generations through cell divisions is necessary. Here, we establish a novel combination of single-cell approaches to trace and quantify the maintenance and inheritance of transcriptional memory in individual cells through repeated stimuli and identify novel regulators of memory. We chose *Saccharomyces cerevisiae GAL1* (galactokinase 1) as a model gene, first, because of its previously characterized reinduction memory (Kundu et al., 2007; Kundu and Peterson, 2009, 2010; Sood and Brickner, 2017; Sood et al., 2017; Stockwell and Rifkin,

2017; Zacharioudakis et al., 2007), in which more Gal1 is expressed in a repeated induction with galactose than in naive cells partly due to changes in chromatin architecture (Kundu and Peterson, 2009; Sood et al., 2017), and second, because asymmetric budding facilitates cell and lineage tracking. Whereas factors regulating Gal1 induction such as Gal4, Gal80, and RSC are well described (Floer et al., 2010; Lohr et al., 1995), the reinduction memory is far less understood. In addition, most studies of Gal1 reinduction memory have so far focused on cell populations, and the inheritance of this memory within single-cell lineages has not been characterized.

Our microfluidic techniques for single-cell capture and observation over time combined with novel analyses allowed us to quantitatively investigate the memory of gene expression in individual cells through divisions (maintenance) as well as transmission from a mother cell (M) to its daughters (Ds; inheritance). Applying this, we (1) identified not only deletions that negatively affect transcriptional memory but also a new gain-of-memory phenotype and (2) dissected their effects on reinduction memory maintenance and inheritance.

RESULTS

Gal1 Transcriptional Memory Is Maintained through Repression in Individual Mothers (Ms)

To characterize the maintenance and inheritance of Gal1 transcriptional reinduction memory in single wild-type (WT) *S. cerevisiae* cells, we used time-lapse microscopy coupled to a microfluidics device to observe the expression of a Gal1-GFP fusion over time in individually tracked cells (Figure 1A; Tables S1 and S2). This custom-made cell-tracking microfluidics device traps individual yeast cells and allows for automated media changes and imaging. Individual cells can be monitored and fluorescence intensities quantified over time through growth up to eight generations. Plotting single-cell traces of Gal1-GFP intensities of yeast cells (and any of their arising progeny) subjected to repeated *GAL1* repression in glucose (glu) and induction in galactose (gal) reveals higher Gal1-GFP intensity in individual cells in the second induction (i2) compared to the first (i1) (Figure 1B). We confirmed that this reinduction memory is also present on the transcriptional level since we observed higher Gal1 RNA levels in i2 by bulk RT-qPCR (Figure S1), in agreement with previous findings in different strain backgrounds (BY4741 and W303 based) (Brickner et al., 2007; Halley et al., 2010). We then compared Gal1 expression in individual Ms (defined here as cells present in both i1 and i2) over time and observed that reinduction memory is higher at all comparable time points within each individual cell throughout all of i2 (Figure 1C). This demonstrates that transcriptional memory is maintained through repression in individual Ms.

For quantitative comparisons of i1 versus i2, we dissected Gal1 expression kinetics into fluorescence intensity and delay (time from galactose exposure to detectable Gal1-GPF signal). Since we observed memory from the start to the end of induction (Figure 1C), we compared fluorescent intensities at just a single time point at the end of each induction. We found that >93% of Ms maintain Gal1 reinduction memory according to either measure (Figure 1D, left and center). While there is a significant difference in delay between i1 and i2 (Figure 1D, center), expression rates are similar (Figure 1D, right; for statistical tests and p values, see Table S3). This reveals that reinduction memory maintenance in Ms leads to higher gene expression in i2 mainly due to shorter delay.

Gal1 Transcriptional Reinduction Memory Is Inherited by Naive Daughters (Ds)

Our microfluidics setup allows us to define pedigrees using lineage tracking based on the asymmetric budding of Ms. By establishing pedigrees, we can distinguish maintenance in Ms from the inheritance of reinduction memory into their gal-naive progeny (Ds, defined here as cells born during r2; Figure 2A), which is not possible from bulk population measurements. Naive Ds behaved like their pre-exposed Ms in terms of both intensity (Figure 2A) and delay (Figure 2B), demonstrating the inheritance of transcriptional memory. We then quantified memory inheritance from Ms to Ds by comparing their pairwise expression trajectories. To remove the general trend of cells being induced and expressing Gal1, which results in extremely high correlations even in unrelated cells due to the general induction trend, we calculated partial correlations (PCs) using average Gal1 expression in the population at each time point as the controlling variable. PCs between M-D intensities over time during i2 revealed a 63% median PC between related pairs (M2-D2) compared to no correlation (0%) for random pairs (U M2-D2; Figure 2C). This demonstrates that the capacity for reinduction memory is inherited through cell division and provides novel quantitative measures for memory inheritance applicable to compare memory effects. Overall, our single-cell analysis shows that reinduction memory is established and maintained in Ms, and efficiently transmitted through repression (r2) to their progeny.

The mechanisms underlying Gal1 reinduction memory are unclear and somewhat controversial. Previously, protein carryover from an initial induction has been shown to contribute to Gal1 reinduction memory (Kundu and Peterson, 2010; Zacharioudakis et al., 2007). When gal is available, Gal3 binds and removes the Gal80 repressor from the *GAL1* promoter, allowing the *GAL* genes to be expressed (Lohr et al., 1995). As Gal1 is a paralog of Gal3, it also has the ability to remove the Gal80 repressor; therefore, during reinduction, undegraded Gal1 could contribute to memory. Chromatin structure has also been implicated in reinduction memory, especially during shorter repression intervals (Kundu et al., 2007; Kundu and Peterson, 2009; Sood and Brickner, 2017; Sood et al., 2017; Stockwell and Rifkin, 2017). Chromatin remodeling by Swi2 is involved in Gal1 induction, and deletion of *SWI2* results in a decrease in memory (Kundu et al., 2007). Furthermore, it has been suggested that deletion of the histone H3K4 trimethyltransferase *SET1* could enhance reinduction (Zhou and Zhou, 2011).

We were interested in determining the role of these factors in our media change protocol and microfluidics setup. We replaced the *GAL1* open reading frame (ORF) with GFP and tagged *GAL3* with a C-terminal mCherry to observe their expression during a microfluidic memory experiment. Our results show that cells that reinduce GFP the highest from the *GAL1* promoter are not

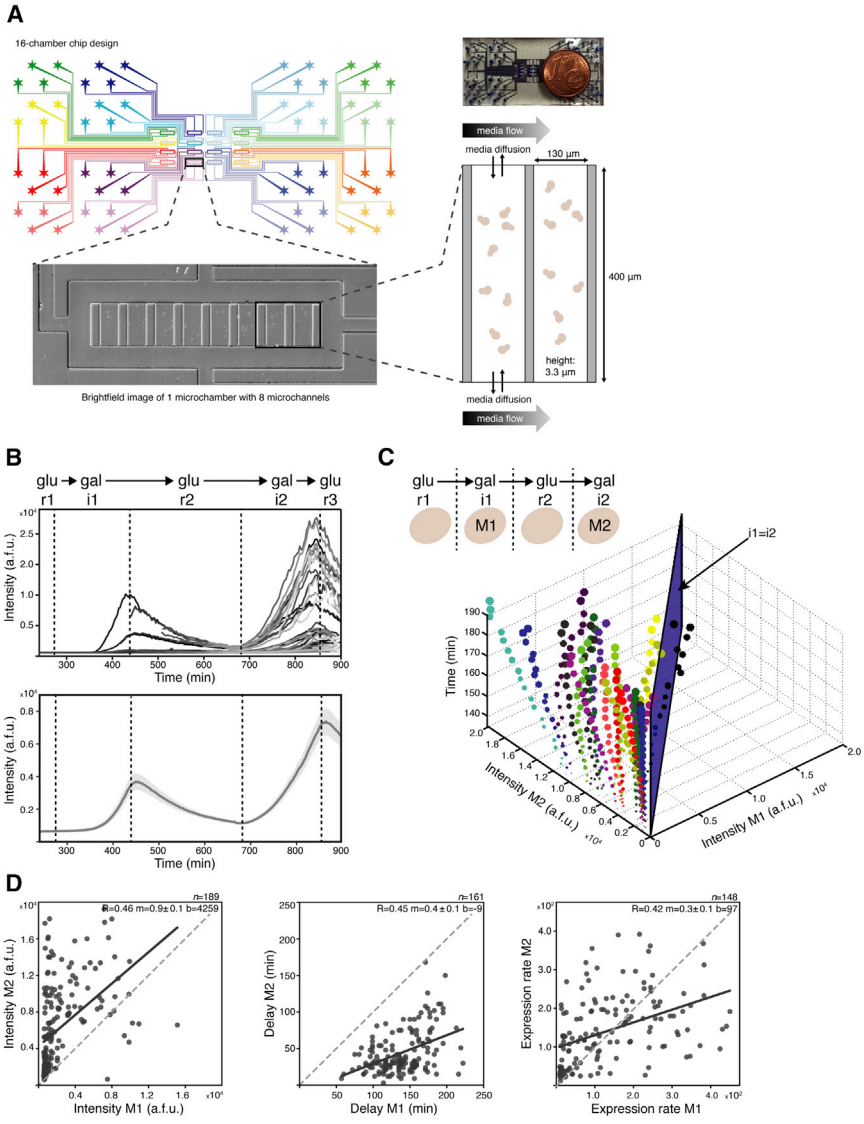

Figure 1. Quantification of Gal1 Memory in Single Cells over Time

(A) Cell- and lineage-tracking microfluidics chip design. The chip is designed with 16 fully independent microchambers to allow up to 16 different strains or conditions to be measured simultaneously with precise time-controlled media changes. Each microchamber contains 8 microchannels in which individual yeast cells can be trapped and maintained in a single plane during growth, enabling subsequent segmentation and expression quantification. The design is compatible with both phase contrast and fluorescence imaging of individual yeast cells with cell and lineage tracking for at least 7 cell divisions. See also Tables S1 and S2.

(B) Top: single-cell traces of Gal1-GFP intensity. Yeast cells were subjected to repeated galactose inductions (gal; i1 and i2, induction 1 and 2, respectively) and glucose repressions (glu; r1, r2, and r3, repression 1, 2, and 3, respectively) during a memory time-lapse imaging experiment using single-cell tracking microfluidics. Individual cells have Gal1 memory (i.e., they express more Gal1 in i2 compared to i1) (representative experiment). Bottom: Gal1 expression population mean (solid line) ± 95% confidence intervals (shaded area) shows that on average the population (including progeny) shows Gal1 memory. See also Figure S1.

(C) Single mother cells (Ms) express more Gal1 at each time point during i2 in comparison with the corresponding time point in i1. M1 and M2 represents the same M in i1 and i2, respectively. Each color represents a single M, with increasing dot size according to time from induction start. Any time point for each cell that falls to the left of the i1 = i2 plane indicates memory (representative experiment).

(D) Left: 93% of Ms have memory according to Gal1 intensity at induction end. M1 and M2 represents the same M in i1 and i2, respectively. Center: 100% of Ms have memory according to delay until detectable Gal1 expression. Right: Gal1 expression rate (see Method Details) in wild-type (WT) Ms is similar during i1 and i2. WT M memory maintenance is due to shorter delay, not increased expression rate, which results in increased intensity in i2.

For statistical tests and p values, see Table S3.

the ones with the highest Gal3 levels before reinduction (Figure S2A). Given that *GAL1* is deleted in these cells, and high Gal3 protein levels are not correlated with increased memory, we next investigated whether any protein expression during i1 is essential for reinduction memory. To address this, cells were induced with gal while simultaneously inhibiting protein translation with cycloheximide (CHX) during i1 such that Gal1 mRNA could be transcribed without translation of the Gal1 protein (and any other nascent protein). In CHX-treated, gal-induced cells, we observed Gal1 mRNA expression but no detectable Gal1-GFP protein during i1, and still witnessed reinduction memory in these cells in i2 (Figures 2D, S2B, and S2C). Finally, we addressed whether reinduction memory transmittance from M to D and hence the number of cell divisions during repression "dilutes" M memory. Ms maintain their gene expression memory independently of the number of progeny produced, signifying that dilution of i1-expressed proteins does not influence i2 induction intensities, and therefore memory (Figure 2E).

These results and other recent findings (Cerulus et al., 2018; Sood and Brickner, 2017; Sood et al., 2017) suggest that, besides the established *trans*-acting proteins (Zacharioudakis et al., 2007), chromatin components could be implicated in Gal1 transcriptional memory in our setup. Indeed, the deletion of *SWI2* in our Gal1-GFP reporter strain resulted in a decrease in memory, recapitulating previous findings on the role of this chromatin remodeler in Gal1 memory (Figure S2D, left). The deletion of *SET1* resulted in high expression during not only reinduction, as reported previously (Zhou and Zhou, 2011), but also the

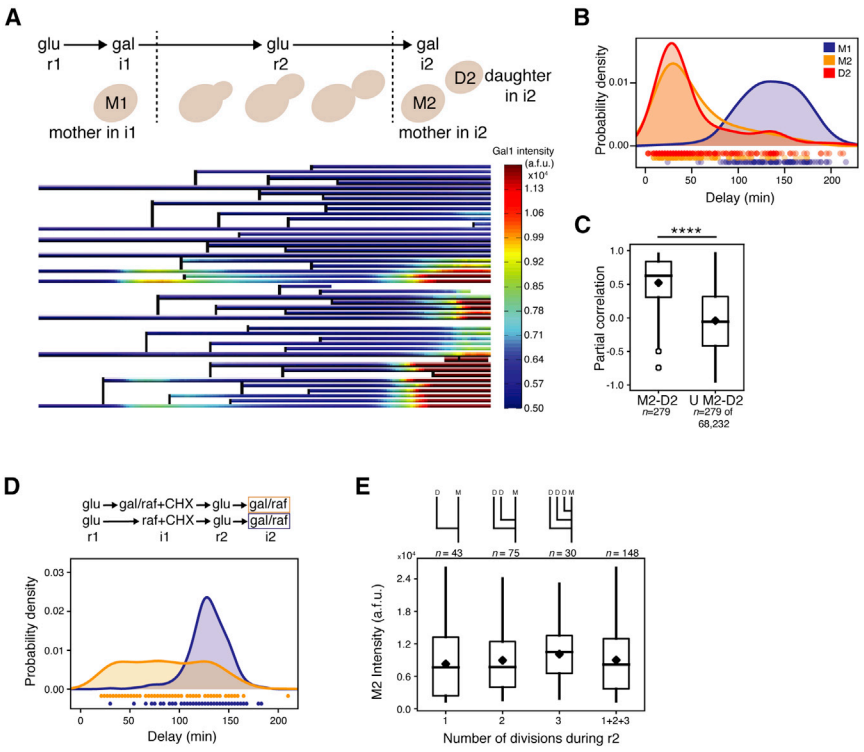

Figure 2. Gal1 Memory Maintenance in Ms and Inheritance in Daughter Cells (Ds)

(A) Gal1 intensity heatmap overlaid on a pedigree shows similar expression patterns between related cells. M induction is detected during both i1 and i2 (M1 and M2, respectively), while only gal-naive Ds born during r2 are analyzed for inheritance in i2.

(B) Unexposed progeny inherit Gal1 memory from pre-exposed Ms according to Gal1 delay. Gal-naive Ds (D2, n = 326) born from pre-exposed Ms have significantly shorter delays in i2 than their Ms in i1 (M1, n = 122), and are indistinguishable from their Ms in i2 (M2, n = 140), indicating memory inheritance.

(C) Related pairs of cells within the same induction (i2) behave more similarly than unrelated cells. To remove the general trend of Gal1 induction, partial correlations (PCs) were calculated. Significantly higher (63%) PCs between related pairs of Ms and Ds during i2 (M2-D2) compared to unrelated pairs (0%, U M2-D2) indicates that Gal1 expression is well correlated over many time points and memory is inherited by Ds.

(D) Protein synthesis during the initial gal induction (i1) is not solely responsible for memory. WT yeast were grown in a microfluidics device in raffinose (raf; non-inducing control, n = 216) or gal/raf medium (n = 177) during i1 in the presence of cycloheximide (CHX) to prevent translation. Following glu repression (r2), all of the cells were induced with gal/raf in i2. Delays until Gal1 expression in i2 show that cells previously exposed to gal reinduce significantly faster than cells naive for gal, even if translation is blocked in i1. See also Figures S2A–S2C.

(E) Cell division does not decrease M memory. Intensity distribution of M intensities in i2 (M2) is not different between Ms that have divided 1, 2, or 3 times (a maximum of 3 progeny can be born during r2), demonstrating that cell division does not significantly decrease mother memory.

For statistical tests and p values, see Table S3.

initial induction. This indicates a general effect of *set1Δ* on Gal1 expression and therefore not a memory-specific phenotype (Figure S2D, right). This could be due to differences in the media changes that affect the extent of *GAL1* repression (Stockwell et al., 2015) or because previous studies analyzed shorter timescales (Zhou and Zhou, 2011). The above work prompted us to systematically screen for chromatin factors that can affect the maintenance and/or inheritance of memory, resulting in an overall loss- or gain-of-reinduction memory in our microfluidics setup in comparison to WT.

Deletion of *CIT1* and *SET3* Cause Loss of Memory, While *ELP6* Deletion Results in a Gain-of-Memory Phenotype

To identify novel chromatin-related loss- and gain-of-memory effectors in an unbiased approach, we screened a library of 567 knockout strains harboring the Gal1-GFP reporter and a single gene knockout (Figure 3A; Table S4) focused on non-essential chromatin-related factors. This library was produced by SGA (synthetic genetic array), a method for semi-automated large-scale genetic manipulation. SGA involves mating the haploid Gal1-GFP reporter strain with a library of deletions in the opposite mating type background to produce diploids, followed by sporulation and selection of haploids containing both the reporter and a single gene deletion. We used a high-throughput microfluidics platform (Dénervaud et al., 2013) with 1,152 chambers for simultaneous screening of each mutant strain in duplicate (and multiple WT replicates), with automated media changes and a segmentation pipeline for single-cell analysis (Figures S3A–S3C).

Based on single-cell Gal1 expression profiles, we observed higher expression in i2 in the WT, validating the presence of transcriptional reinduction memory in this microfluidics setup (Figure 3B). With this high-resolution and high-throughput approach, we systematically compared strains and identified outliers with altered behavior in expression (Figure 3C, left) and/or delay (Figure 3C, right). We hypothesized that the deletion of some Gal1 transcriptional machinery components may affect Gal1 induction, and found that the inactivation of RSC (remodeling the structure of chromatin) (Floer et al., 2010) (data not shown) or the Gal4 transcriptional activator resulted in generally poor induction, not specific to reinduction. To identify outliers specifically during i2 based on fluorescence intensity, we compared the average fluorescence for each strain in each induction against the average fluorescence of all other strains at that time point as a more robust measure than comparing to WT only (see Method Details; Figure 3C, left). To identify outliers based on delay, we compared the delay for each strain until 50% of cells were expressing Gal1 in each induction (Figure 3C, right). By applying these measures, we discovered multiple previously unknown loss-of-memory mutants but remarkably also novel gain-of-memory candidates. For 30 candidates, we

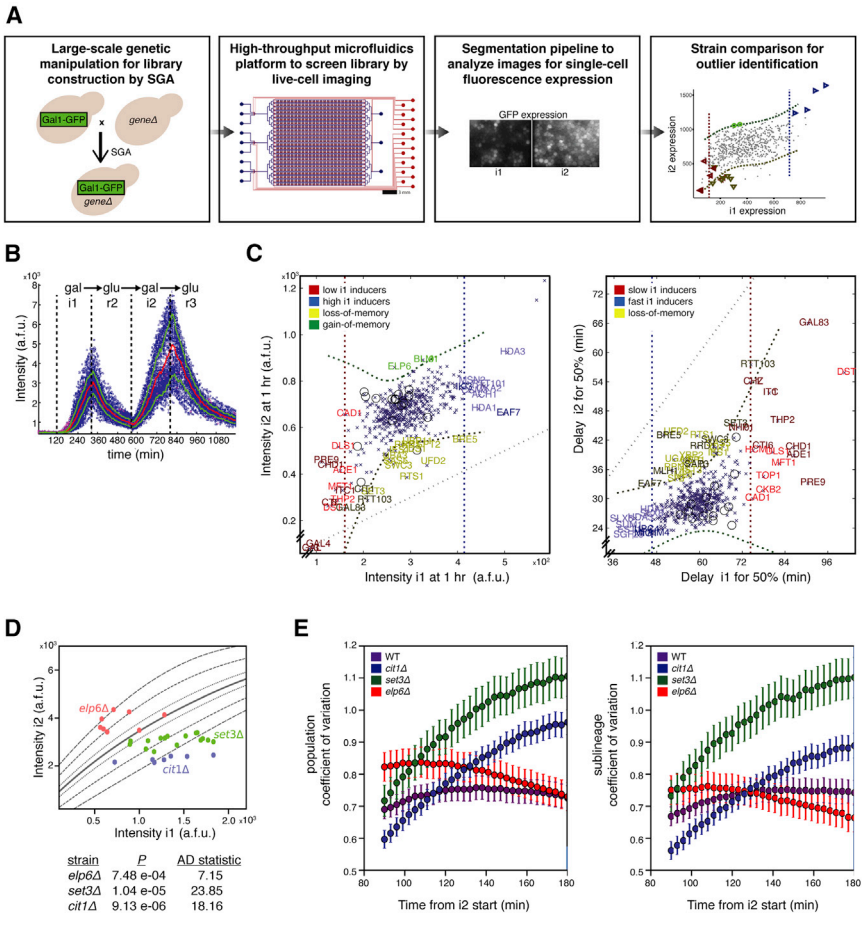

Figure 3. Identification of Loss- and Gain-of-Memory Mutants through a Novel Workflow for High-Throughput Screening

(A) Workflow of screening includes the production of a library of strains harboring a single gene deletion and the reporter of interest using the high-throughput SGA system of library construction (first panel). The strains are then screened in high throughput using a microfluidics device with 1,152 chambers for the automated control of media changes (second panel). Images are processed with an automated segmentation and analysis pipeline (third panel) to identify outliers of interest (dashed lines indicate outlier thresholds [fourth panel]). The high capacity of the microfluidics chip allowed us to test all of the strains in duplicate simultaneously with 3 biological replicates. See also Table S4 and Figures S3A–S3C.

(B) Profile of WT in a high-throughput microfluidics experiment shows memory in the setup. Blue circles represent fluorescence in single cells. Red and green lines represent median and quartiles, respectively.

(C) Detection of outliers of Gal1 memory (yellow and green) according to intensity and population expression delay. Crosses represent individual yeast strains with the Gal1-GFP reporter and a single gene deletion. Open circles represent WT replicates. Dashed lines indicate outlier thresholds. Specifically, Gal1 memory outliers are defined as those that are found within the 2 vertical dashed lines in i1, but outside the 2 horizontal dashed lines in i2. Left: outliers according to mean Gal1 intensity in i1 and i2. Representative outlier plot 1 h after induction start in i1 and i2. Right: outliers according to population expression delay (time until 50% of the population is expressing detectable Gal1).

(D) Comparison of mutants with memory observed in WT yeast at matched induction strengths verifies loss- and gain-of-memory candidates. Lines represent WT induction in i1 and i2 as induction length is varied: mean induction (solid line) and quantile contour lines quantifying variability (dashed lines). Dots represent average induction strengths in i1 and i2 in individual mutant experiments. Anderson-Darling (AD) test statistics confirm that the mutants deviate significantly from the mean WT induction (see Method Details). See also Figures S4A–S4D.

(E) Left: WT and *elp6Δ* have markedly lower variability (coefficient of variation) in Gal1 expression dynamics than *set3Δ* and *cit1Δ*. Circles indicate means and error bars SDs from bootstrapping (×1,000). Right: increased Gal1 delay is a feature of some loss-of-memory cell lineages, resulting in high variability (coefficient of variation) between sublineages, particularly within *set3Δ* but also in *cit1Δ* during i2.

For statistical tests and p values, see Table S3.

recreated knockout strains by homologous recombination and performed independent single-cell tracking microfluidics experiments. This allowed us to validate *set3Δ* and *cit1Δ* as the most striking loss-of-memory mutants and *elp6Δ* as the most robust gain-of-memory mutant (Figures 3D and S4A). We also confirmed these phenotypes at the transcript level (Figure S4B). As shown by comparing mutant strains with WT at equivalent i1 induction levels (Figures 3D and S4A) or thresholding for the same i1 expression level in all strains (Figure S4C, center panel), these loss- or gain-of-memory phenotypes are not simply due to overall impaired or enhanced induction. In line with this, the exclusion of "non-inducers" (Figure S4D) within the loss-of-memory populations did not change their phenotypes (Figure S4C, bottom panel).

Our cell-tracing analysis allows us to quantify and study the variability in Gal1 expression dynamics and to distinguish sublineages within the population. By calculating a coefficient of variation for all of the cells (related and unrelated) in the population, we detected a high population variation specifically in Gal1 reinduction in *set3Δ* and *cit1Δ*, but not WT and *elp6Δ* (Figure 3E, left panel). As increased variability is correlated with slower growth rates (Keren et al., 2015), we compared doubling times (Schmidt et al., 2018) for each strain and found that there are no significant differences between the mutants and WT, except for *cit1Δ*, which actually seems to grow faster ($p = 0.0133$, Mann-Whitney *U* with Bonferroni correction). Therefore, slower growth rates are not the underlying source of variability in the loss-of-memory mutants. Rather, by comparing coefficients of variation between groups of related cells within each strain (sublineages), we found that this variability is partially due to particular sublineages of non-inducers or very slow inducers in *set3Δ* and *cit1Δ* (Figure 3E, right panel). This observation points to an inheritable inducing state. While Set3, a member of a histone

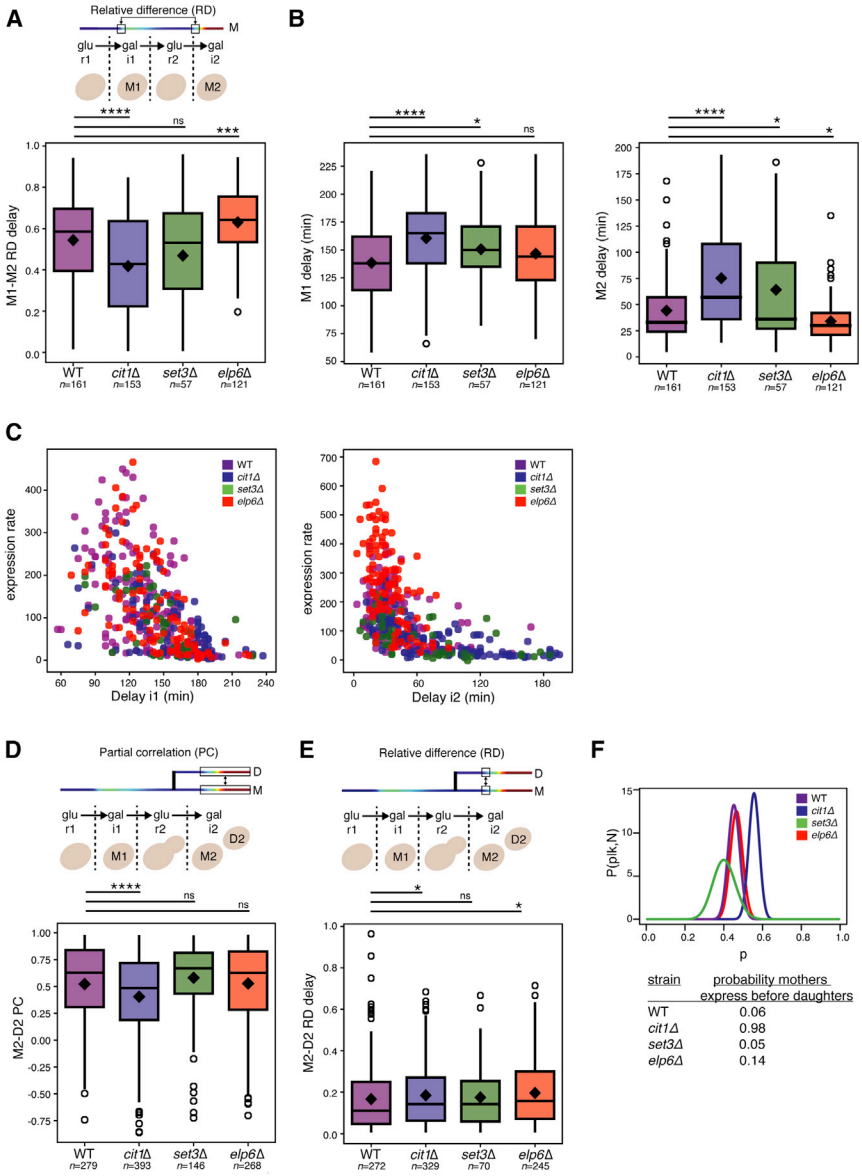

Figure 4. Dissection of Mutant Effects on Maintenance and Inheritance of Gal1 Memory

(A) Loss- and gain-of-memory mutants affect maintenance of M memory. M1-M2 relative difference (RD) in the delay reveals that loss-of-memory mutant *cit1Δ* has significantly lower RD than WT, while gain-of-memory *elp6Δ* is significantly higher, indicating that these phenotypes are at least in part due to an effect on the maintenance of M memory from i1 to i2.

(B) Left: loss-of-memory *set3Δ* and *cit1Δ* have longer delays than WT in i1. Gain-of-memory *elp6Δ*, however, has similar delays as WT in i1. Right: *elp6Δ* has shorter delays in i2, while *set3Δ* and *cit1Δ* have longer delays in i2 than WT.

(C) Left: comparison of expression rates of cells with similar delays shows no major differences between mutants and WT in i1. Right: comparison of *elp6Δ* cells with similar delays as WT reveals an increased expression rate in i2. See also Figure S5.

(D) *cit1Δ* is the only strain with lower M2-D2 PC in i2 in comparison to WT. Low M2-D2 PC in *cit1Δ* suggests that Ms and Ds do not share the same memory.

(E) Increased M2-D2 RDs in *cit1Δ* and *elp6Δ* in comparison to WT reveals higher variability between Ms and Ds.

(F) Posterior distribution functions [P(p|k,N)] of strains to determine bias toward Ms expressing earlier than Ds in i2 (p). Shown are the probabilities [P(p|k,N)] that a deviation from neither M nor D expressing first (p = 0.5) is significant. *cit1Δ* shows a 98% probability that Ms express before Ds (p > 0.5), while in all of the other strains, the probability for such preference is negligible, suggesting that *cit1Δ* has a defect in the inheritance of memory.

For statistical tests and p values, see Table S3.

deacetylase complex, has previously been implicated in decreased Gal1 reinduction (Kim et al., 2012), Cit1 and Elp6 represent novel regulators of Gal1 memory. Cit1 is a factor using mitochondrial acetyl-coenzyme A (CoA) (Kim et al., 1986) and Elp6 is a subunit of the so-called "Elongator" (Elp) complex (Krogan and Greenblatt, 2001). Thus, our screening identified new pathways modulating transcriptional reinduction memory and even an unanticipated gain-of-memory phenotype.

Deletion of *CIT1* Results in Asymmetric Memory Inheritance

Next, applying the quantitative measures we developed for WT yeast (see above), we used our pedigree analysis to dissect how these mutations specifically affect reinduction memory maintenance and/or inheritance. We first focused on memory maintenance effects by examining the relative difference (RD) between delay in expression in i1 and i2 of the same M (M1-M2), which was calculated by dividing the absolute value of the difference in delays by the sum of the delays. We observed that *elp6Δ* strains exhibit a higher RD in delay, while *cit1Δ* has a lower RD in comparison to WT (Figure 4A). This demonstrates that effects on transcriptional reinduction memory maintenance in Ms contribute to both gain-of-memory and loss-of-memory phenotypes. In general, *set3Δ* and *cit1Δ* Ms have longer delays than WT, while in *elp6Δ*, we observed no effects on i1 delay, but significantly shorter i2 delays than WT (Figure 4B). Due to positive feedback in the Gal network, the expression rate depends on the delay; cells that start expressing earlier have a higher expression rate in comparison to cells that start expressing later. To eliminate differences due to the delay, we compared expression rates of mothers with similar delays and observed no effects on the expression rate in *set3Δ* and *cit1Δ* in either i1 or i2 (Figure 4C). Comparison of *elp6Δ* Ms with similar delays as WT, however, reveals similar expression rates in i1 but an increased expression rate in i2 (Figure 4C).

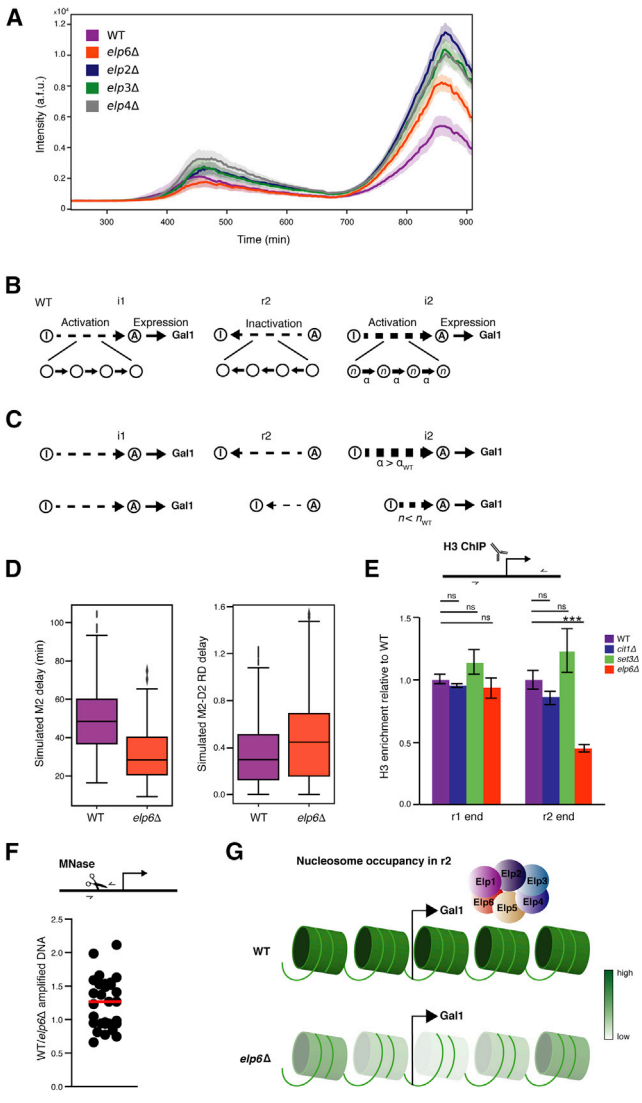

Figure 5. Analysis of *elpΔ*-Mediated Gain-of-Memory Effect

(A) Deletion of individual Elp complex members results in gain-of-memory. Shown are Gal1 expression population means (solid lines) ± 95% confidence intervals (shaded areas) from microfluidics data of single *ELP* complex member deletions. Deletion of *ELP2*, *ELP3*, or *ELP4* recapitulates the gain-of-memory results observed in *elp6Δ*, indicating that gain-of-memory results from a dysfunctional Elp complex. See also Figure S6A.

(B) Delay model. Induced cells in i1 transition from an inactive *GAL1* promoter state (I) to an active state (A) in sequential steps, leading to Gal1 expression. During repression (r2), the *GAL1* promoter is inactivated. Shorter WT delay can be envisioned as coming from an increased activation rate α.

(C) Gain-of-memory hypotheses predict shorter delays due to (i) faster activation rates ($\alpha > \alpha_{WT}$) or (ii) fewer activation steps ($n < n_{WT}$).

(D) Fitting a stochastic delay model to the single-cell data shows that fewer activation steps with unchanged activation rates can explain both a shorter delay and a broader M-D RD distribution in i2, as is observed for the *elp6Δ* gain-of-memory phenotype (see Figures 4B and 4E).

(E) ChIP reveals decreased histone H3 enrichment at the *GAL1* promoter in *elp6Δ* at the end of r2. Samples were collected at the end of r1 and r2 and H3 IPs at the *GAL1* promoter (arrow, transcription start site [TSS]) were quantified by qPCR, with mutants normalized to WT. Error bars indicate SDs for 2 technical replicates each from 2 biological replicates; representative experiments verified by 3 additional biological replicates.

(F) Nuclease sensitivity assays show higher susceptibility to MNase digestion in *elp6Δ* compared to WT at the end of r2. Samples were collected at the end of r2 and digested with MNase, and then protected DNA was amplified by qPCR. Individual dots represent the ratio of WT to *elp6Δ* amplified DNA. Shown are 29 digestions from 4 biological replicates, with the median ratio (1.27) represented by the red bar. The higher median ratio of WT to *elp6Δ* indicates that the *elp6Δ* samples contain less protected DNA than WT and that *elp6Δ* chromatin at the *GAL1* promoter at the end of r2 is more susceptible to MNase digestion.

(G) Schematic for proposed gain-of-memory mechanism in Elp mutants by reduced nucleosome occupancy during repression in r2, resulting in faster reinduction in i2.

For statistical tests and p values, see Table S3.

These data, corroborated by linear fits of M1-M2 intensity scatterplots (Figure S5), support a reinduction memory model in which gain-of-memory affects both the delay and expression rate during memory maintenance in Ms, whereas loss-of-memory affects only the delay in i2. This indicates that both types of mutants act through the maintenance of reinduction memory in the Ms.

To investigate specific effects on the inheritance of memory into Ds, we compared Ms with their respective Ds in i2 (M2-D2), again using PC. This analysis revealed that *cit1Δ* has a significantly lower M2-D2 PC (Figure 4D), indicating that Ms and Ds do not follow the same trajectory of Gal1 expression. In addition, *cit1Δ* Ms and Ds have a high relative delay difference (RD, Figure 4E)—in other words, Gal1 expression delays differ within each M-D pair. While both the PC and RD can reveal differences between Ms and Ds, neither measure indicates whether there is indeed a defect in D memory inheritance; therefore, we used Bayesian statistics with posterior distribution functions to determine whether there is any bias in Ms or Ds expressing first. We found that *cit1Δ* is the only strain with a probability skewed toward Ms expressing Gal1 before their Ds in i2 (Figure 4F). This suggests that loss of Cit1, unlike our other loss-of-memory mutant *set3Δ*, results in a defect in memory inheritance. This unveils the first mutant with a described asymmetric transcriptional reinduction memory inheritance, exacerbating the loss-of-memory phenotype.

Gain-of-Memory Is a Property of Elp Complex Members, Resulting from Incomplete Nucleosome Reincorporation during Repression

We then focused on the intriguing gain-of-memory phenotype we discovered in *elp6Δ*. Elp6 is part of a 6-member Elp complex of proteins (Krogan and Greenblatt, 2001). Independent deletions of 3 other non-essential Elp subunits also exhibited memory enhancement (Figures 5A and S6A), demonstrating that this gain-of-memory phenotype is a property of a dysfunctional Elp complex. Our cell tracking allowed us to further analyze the *elp6Δ* gain-of-memory phenotype according to expression levels in i1. We sorted cells into three i1 expression bins—low, medium, and high—and found that a stronger i1 leads to an even stronger *elp6Δ* gain-of-memory phenotype in comparison to WT (Figure S6B). Further dissection of *elp6Δ* tracking and lineages revealed that *elp6Δ* has a discernible effect on delay differences (RD) between Ms and Ds in i2 (Figure 4E), but no

effect on the M-D induction dynamics (PC; Figure 4D) or bias toward Ms or Ds expressing first (Figure 4F). This lack of bias and no effect on PC indicates that the observed M-D delay differences are not due to altered inheritance. Considering the previous known links of the Elp complex with chromatin and transcription (Li et al., 2009; Svejstrup, 2007), we hypothesized that its effects could stem from changes in promoter activation before Gal1 detection.

To explore how a chromatin-based gain of transcriptional reinduction memory could contribute to M-D delay differences, we devised a minimal model for Gal1 expression. We envisioned gene activation as a series of sequential activation steps (i1; Figure 5B), including chromatin-related processes such as nucleosome remodeling, histone modifications, and transcriptional machinery recruitment, leading to *GAL1* promoter activation and expression. Soon after glu-induced repression, preinitiation complex components and RNA polymerase II are not detected at the *GAL1* promoter (Kundu et al., 2007), suggesting that cells cascade back to an inactive state (r2; Figure 5B) and that WT memory may be due to increased activation rates in i2. We considered two gain-of-memory hypotheses (Figure 5C) in which the manipulation of chromatin-related processes could lead to shorter delays, and hence the gain-of-memory phenotype that we observed in *elp6Δ* (Figure 4B, right panel): either the rates of the individual activation steps in i2 are even larger in *elp6Δ* than in WT or *elp6Δ* requires fewer reactivation steps than WT (Figure 5C). We tested which of the two hypotheses is more likely with a quantitative stochastic model of stepwise activation. Our model consists of two parameters: the number of activation steps n and the activation rate α (see Method Details). We found that a model in which the number of activation steps is reduced in *elp6Δ* while the activation rate α is unchanged can explain both effects observed in the data: a shorter delay in *elp6Δ* and a larger relative M-D difference (Figure 5D). Mechanistically, gain-of-memory and faster reinduction based on a reduced number of reinduction steps could be explained by *GAL1* being "primed" for reactivation, for example, by altered nucleosome occupancy. To test for this possibility, we performed chromatin immunoprecipitation (ChIP) for histone H3 at *GAL1*. We found that H3 levels at *GAL1* at the end of r2 in *elp6Δ* remain lower than in WT (Figure 5E). To further substantiate this finding, we compared nuclease sensitivity at the *GAL1* promoter in WT and *elp6Δ* at the end of r2 and found that *elp6Δ* chromatin can be more susceptible to nuclease digestion compared to WT (Figure 5F). Both the results from the H3 ChIP and the nuclease sensitivity assay strongly suggest that incomplete nucleosome reincorporation during repression, which in turn maintains an open chromatin state that is permissive for faster Gal1 reinduction, could contribute to the unexpected gain-of-memory phenotype. This implies a potential novel function for the Elp complex in facilitating nucleosome restoration during repression, which is in line with previous findings on Elp complex involvement in nucleosome assembly (Li et al., 2009).

DISCUSSION

Our combination of experimental single-cell approaches, pedigree analysis, and mathematical modeling allowed us to discover new loss-of-memory and gain-of-memory effectors. It also highlights the powerful nature of single-cell tracking approaches to tackle fundamental biological questions.

For the memory factors Elp6, Cit1, and Set3, we applied pedigree analysis to dissect their effects on the maintenance of reinduction memory in Ms through cell divisions and effects on inheritance into Ds. We found that these mutants can affect the kinetics of the *GAL1* promoter reaching its fully active (or repressed) state and alter the timing of transcription during reinduction. We were surprised to identify a gain-of-memory mutant, and thus focused our further studies on this phenotype. The Elp complex was originally identified as playing a role in transcriptional elongation along with RNA polymerase II (Otero et al., 1999). However, it has since been implicated in various cellular processes, including tRNA modification and histone acetylation, nucleosome assembly, and transcription (Chen et al., 2011; Esberg et al., 2006; Li et al., 2009; Rahl et al., 2005; Svejstrup, 2007), although its exact function is still unclear. This makes understanding its precise molecular role in Gal1 memory challenging. Elp components have been shown to be present at the *GAL1* locus (Santisteban et al., 2011). Since histone acetyltransferase activity through its Elp3 subunit has been described (Winkler et al., 2002; Wittschieben et al., 1999), it is possible that disruption of the complex and its potential histone-modifying activity could affect histone deposition at *GAL1*, leading to the faster reinduction that we observed. In line with this, the incorporation of a partially unwound H2A.Z-containing nucleosome by the RSC complex at the *GAL1* promoter facilitates Gal4 transcriptional activator binding, nucleosome loss, and faster induction (Floer et al., 2010).

We propose that the Elp complex may directly or indirectly alter chromatin organization at *GAL1* by affecting nucleosome restoration during repression, thereby priming *GAL1* for reactivation (Figure 5F) and contributing to the gain-of-memory phenotype. This is supported by our ChIP and nuclease sensitivity data and mathematical modeling. A prediction from this would be that *elp* mutants may allow a cell to tolerate longer repression times, without losing transcriptional reinduction memory, and enable memory-storage capabilities at other inducible Elp complex targets in an *elpΔ* background. In higher eukaryotes, a combination of altered nucleosome occupancy (as observed in our yeast model) and/or the absence of repressive histone modifications during repression could achieve a similar gain-of-memory phenotype.

While the mechanisms underlying transcriptional memory have been elusive, chromatin does seem to play a role. We observed memory independent of Gal1 and not correlated with Gal3 levels in our approach and found that deletion of the chromatin remodeling factor *SWI2* results in reduced memory, pointing to a role for chromatin. The roles of various factors are, however, affected by the media change protocols, especially by the length of repression (Kundu and Peterson, 2010; Stockwell et al., 2015). For example, *set1Δ* did not show a memory-specific phenotype as was previously suggested, but rather an increase in Gal1 expression in both inductions in our media change protocol in which we have the same length of glucose repression before each induction.

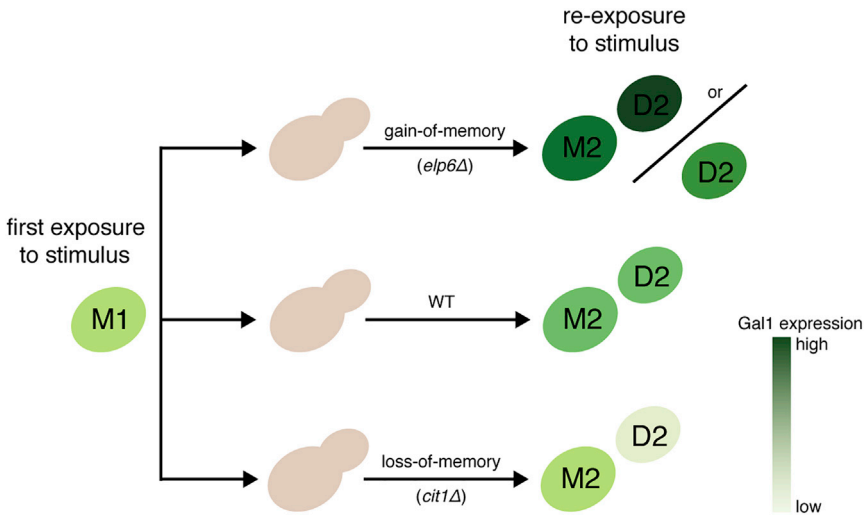

Figure 6. Schematic Highlighting Identified Defects in the Maintenance and Inheritance of Memory

WT Ms establish and maintain a transcriptional memory during exposure to a stimulus (gal), resulting in higher expression (indicated by darker color) during re-exposure. Unexposed Ds inherit a memory potential similar to that of their Ms. The mutants identified in our screen have different effects on maintenance and inheritance of memory. Gain-of-memory in *elp6Δ* results in increased M memory, and while *elp6Δ* Ds also generally have gain-of-memory compared to WT cells, there is variability in memory inheritance from their Ms. However, *cit1Δ* loss-of-memory results in decreased M memory, with an even stronger phenotype in Ds, resulting in a pattern of asymmetric memory.

Our screening revealed that deletion of *SET3* results in loss-of-memory, a phenotype that was also observed previously (Kim et al., 2012); however, *set3Δ* was only investigated in bulk populations and its effects on memory maintenance and inheritance were not studied. It is plausible to assume a role of its histone deacetylase activity in the loss-of-memory phenotype (Kim et al., 2012). Our screening also identified Cit1 as a novel regulator of Gal1 reinduction memory. Cit1 protein levels have been shown to positively correlate with shorter delays during Gal1 reinduction (Cerulus et al., 2018). This is in line with our finding that *CIT1* deletion results in longer delays during reinduction, which leads to its loss-of-memory phenotype. We found that Cit1 has a striking effect on memory inheritance, and *cit1Δ* Ms induce Gal1 before their Ds. Inheritance analyses, such as those described herein, require images with high temporal resolution as in our setup, which can affect cellular well-being (e.g., growth rates). Therefore, it is vitally important to consistently compare experimental strains to a corresponding WT control, as we did in our studies. It is unclear why *cit1Δ*, unlike our other loss-of-memory mutant *set3Δ*, results in such impaired transcriptional memory inheritance—perhaps the compromised metabolic state in *cit1Δ* (Cerulus et al., 2018) is better tolerated by mother cells.

Overall, our inheritance analysis suggests that there are distinct mechanisms of establishment and inheritance of transcriptional reinduction memory in yeast cells. It supports a model in which gain-of-memory affects both the delay and expression rate during memory maintenance in Ms, whereas loss-of-memory likely affects only delay in i2. We observed that inheritance can be asymmetric with an even stronger loss of memory in the Ds, as is the case in *cit1Δ*, or inheritance can be a symmetric gain-of-memory with high variability, as observed in the Ds of *elp6Δ* (Figure 6).

The memory mutants we identified function by affecting a combination of resources and chromatin-related processes involving nucleosomes and histone modifications directly or indirectly and provide us with novel effectors of Gal1 memory. This suggests that heritable chromatin states can contribute to reinduction memory in addition to protein-based feedback loops (Kundu and Peterson, 2010; Stockwell and Rifkin, 2017; Zacharioudakis et al., 2007). The top 30 factors identified from our high-throughput screening can regulate a wide range of target genes beyond *GAL1*. This opens up the possibility that transcriptional memory occurs at many more genes that can be induced and also in other organisms in which these factors are conserved. The existence of a gain-of-memory phenotype hints that there may be an optimal range of transcriptional memory. Whereas some memory can offer a competitive advantage in nutrient-limited environments, enhanced memory may result in a loss of bet-hedging strategies necessary to deal with repeated stresses.

It has become clear that studying whole populations of cells has so far limited our understanding of transcription dynamics and, in particular, the inheritance of transcriptional states. Our approach relies on the implementation of microfluidic technologies for both high-throughput screening and in-depth lineage analyses on the inheritance of transcriptional/chromatin states. More generally, the microfluidics technologies are not limited to studies of transcription, but will also be useful to studies of cell size, cell cycle, aging, and more. With rapidly developing microfluidics technologies and the discovery of feasible approaches to reporter and mutant library construction, we expect that our workflow can now be applied to various organisms, including mammalian cells, which will open up avenues to understand human cell behavior—in particular, towards disease tolerance and cell heterogeneity.

STAR★METHODS

Detailed methods are provided in the online version of this paper and include the following:

- KEY RESOURCES TABLE
- RESOURCE AVAILABILITY
  - Lead Contact
  - Materials Availability
  - Data and code availability
- EXPERIMENTAL MODEL AND SUBJECT DETAILS

SUPPLEMENTAL INFORMATION

Supplemental Information can be found online at https://doi.org/10.1016/j.molcel.2020.04.016.

ACKNOWLEDGMENTS

We thank Youlian Goulev for support on the cell-tracking microfluidics setup and Michael Strasser for guidance on the modeling. We thank Matthias Meurer, Michael Knop, Ben Timney and Michael Rout for the plasmids, and Charlie Boone for yeast strains. Work in the R.S. laboratory was supported by the Deutsche Forschungsgemeinschaft (DFG) through SFB 1064 (Project-ID 213249687) and SFB 1309 (Project-ID 325871075), the EpiTrio consortium, the AmPro program (ZT0026), and the Helmholtz Gesellschaft. A European Research Council (ERC) starting grant, no. 260797, supported work in the A.K. laboratory. P.B. is a Marie Curie International Incoming Fellowships (IIF) fellow and an EMBO Long-Term Fellowships (LTF) fellow. J.B. and S.J.M. were supported by a SystemsX.ch grant DynamiX-RTD (2008/005) and École Polytechnique Fédérale de Lausanne (EPFL). G.C. was supported by grant no. ANR-10-LABX-0030-INRT, a French State fund managed by the Agence Nationale de la Recherche under the frame program Investissements d'Avenir ANR-10-IDEX-0002-02.

AUTHOR CONTRIBUTIONS

P.B., A.K., and R.S. conceived the study. E.S. and A.K. constructed the reporter library. J.B. performed the high-throughput microfluidic screen, and J.B. and S.M. designed the experiment, analyzed the data, and identified the memory mutant candidates. P.B., D.A.-G., and I.K. performed the cell-tracking microfluidics time-lapse experiments and processed the data. G.C. developed the cell-tracking microfluidics and the cell-tracking image analysis pipeline. P.B., D.A.-G., C.M., and N.B.B. analyzed the cell-tracking microfluidics data. D.A.-G., P.B., and C.M. developed the model and performed the corresponding analysis. S.M., G.C., T.H., N.B.B., and C.M. critically revised the manuscript. P.B., A.K., and R.S. wrote the manuscript.

DECLARATION OF INTERESTS

The authors declare no competing interests.

Received: August 30, 2019
Revised: February 15, 2020
Accepted: April 15, 2020
Published: May 8, 2020

REFERENCES

Avramova, Z. (2015). Transcriptional 'memory' of a stress: transient chromatin and memory (epigenetic) marks at stress-response genes. Plant J. *83*, 149–159.

Berry, S., Dean, C., and Howard, M. (2017). Slow Chromatin Dynamics Allow Polycomb Target Genes to Filter Fluctuations in Transcription Factor Activity. Cell Syst. *4*, 445–457.e8.

Brachmann, C.B., Davies, A., Cost, G.J., Caputo, E., Li, J., Hieter, P., and Boeke, J.D. (1998). Designer deletion strains derived from Saccharomyces cerevisiae S288C: a useful set of strains and plasmids for PCR-mediated gene disruption and other applications. Yeast *14*, 115–132.

Brickner, D.G., Cajigas, I., Fondufe-Mittendorf, Y., Ahmed, S., Lee, P.C., Widom, J., and Brickner, J.H. (2007). H2A.Z-mediated localization of genes at the nuclear periphery confers epigenetic memory of previous transcriptional state. PLoS Biol. *5*, e81.

Bryant, G.O., Prabhu, V., Floer, M., Wang, X., Spagna, D., Schreiber, D., and Ptashne, M. (2008). Activator control of nucleosome occupancy in activation and repression of transcription. PLoS Biol. *6*, 2928–2939.

Cerulus, B., Jariani, A., Perez-Samper, G., Vermeersch, L., Pietsch, J.M., Crane, M.M., New, A.M., Gallone, B., Roncoroni, M., Dzialo, M.C., et al. (2018). Transition between fermentation and respiration determines history-dependent behavior in fluctuating carbon sources. eLife *7*, e39234.

Chen, C., Huang, B., Eliasson, M., Rydén, P., and Byström, A.S. (2011). Elongator complex influences telomeric gene silencing and DNA damage response by its role in wobble uridine tRNA modification. PLoS Genet. *7*, e1002258.

Costanzo, M., Baryshnikova, A., Bellay, J., Kim, Y., Spear, E.D., Sevier, C.S., Ding, H., Koh, J.L., Toufighi, K., Mostafavi, S., et al. (2010). The genetic landscape of a cell. Science *327*, 425–431.

D'Urso, A., and Brickner, J.H. (2017). Epigenetic transcriptional memory. Curr. Genet. *63*, 435–439.

Dénervaud, N., Becker, J., Delgado-Gonzalo, R., Damay, P., Rajkumar, A.S., Unser, M., Shore, D., Naef, F., and Maerkl, S.J. (2013). A chemostat array enables the spatio-temporal analysis of the yeast proteome. Proc. Natl. Acad. Sci. USA *110*, 15842–15847.

Esberg, A., Huang, B., Johansson, M.J., and Byström, A.S. (2006). Elevated levels of two tRNA species bypass the requirement for elongator complex in transcription and exocytosis. Mol. Cell *24*, 139–148.

Floer, M., Wang, X., Prabhu, V., Berrozpe, G., Narayan, S., Spagna, D., Alvarez, D., Kendall, J., Krasnitz, A., Stepansky, A., et al. (2010). A RSC/nucleosome complex determines chromatin architecture and facilitates activator binding. Cell *141*, 407–418.

Foster, S.L., Hargreaves, D.C., and Medzhitov, R. (2007). Gene-specific control of inflammation by TLR-induced chromatin modifications. Nature *447*, 972–978.

Francis, N.J., and Kingston, R.E. (2001). Mechanisms of transcriptional memory. Nat. Rev. Mol. Cell Biol. *2*, 409–421.

Goulev, Y., Morlot, S., Matifas, A., Huang, B., Molin, M., Toledano, M.B., and Charvin, G. (2017). Nonlinear feedback drives homeostatic plasticity in H_2O_2 stress response. eLife *6*, e23971.

Halley, J.E., Kaplan, T., Wang, A.Y., Kobor, M.S., and Rine, J. (2010). Roles for H2A.Z and its acetylation in GAL1 transcription and gene induction, but not GAL1-transcriptional memory. PLoS Biol. *8*, e1000401.

Iberg-Badeaux, A., Collombet, S., Laurent, B., van Oevelen, C., Chin, K.K., Thieffry, D., Graf, T., and Shi, Y. (2017). A Transcription Factor Pulse Can Prime Chromatin for Heritable Transcriptional Memory. Mol. Cell. Biol. *37*, e00372-16.

Keren, L., van Dijk, D., Weingarten-Gabbay, S., Davidi, D., Jona, G., Weinberger, A., Milo, R., and Segal, E. (2015). Noise in gene expression is coupled to growth rate. Genome Res. *25*, 1893–1902.

Khmelinskii, A., Keller, P.J., Bartosik, A., Meurer, M., Barry, J.D., Mardin, B.R., Kaufmann, A., Trautmann, S., Wachsmuth, M., Pereira, G., et al. (2012).

Tandem fluorescent protein timers for in vivo analysis of protein dynamics. Nat. Biotechnol. *30*, 708–714.

Kim, K.S., Rosenkrantz, M.S., and Guarente, L. (1986). Saccharomyces cerevisiae contains two functional citrate synthase genes. Mol. Cell. Biol. *6*, 1936–1942.

Kim, T., Xu, Z., Clauder-Münster, S., Steinmetz, L.M., and Buratowski, S. (2012). Set3 HDAC mediates effects of overlapping noncoding transcription on gene induction kinetics. Cell *150*, 1158–1169.

Klinger, E., Rickert, D., and Hasenauer, J. (2018). pyABC: distributed, likelihood-free inference. Bioinformatics *34*, 3591–3593.

Krogan, N.J., and Greenblatt, J.F. (2001). Characterization of a six-subunit holo-elongator complex required for the regulated expression of a group of genes in Saccharomyces cerevisiae. Mol. Cell. Biol. *21*, 8203–8212.

Kundu, S., and Peterson, C.L. (2009). Role of chromatin states in transcriptional memory. Biochim. Biophys. Acta *1790*, 445–455.

Kundu, S., and Peterson, C.L. (2010). Dominant role for signal transduction in the transcriptional memory of yeast GAL genes. Mol. Cell. Biol. *30*, 2330–2340.

Kundu, S., Horn, P.J., and Peterson, C.L. (2007). SWI/SNF is required for transcriptional memory at the yeast GAL gene cluster. Genes Dev. *21*, 997–1004.

Kushnirov, V.V. (2000). Rapid and reliable protein extraction from yeast. Yeast *16*, 857–860.

Kyriakou, D., Stavrou, E., Demosthenous, P., Angelidou, G., San Luis, B.J., Boone, C., Promponas, V.J., and Kirmizis, A. (2016). Functional characterisation of long intergenic non-coding RNAs through genetic interaction profiling in Saccharomyces cerevisiae. BMC Biol. *14*, 106.

Li, Q., Fazly, A.M., Zhou, H., Huang, S., Zhang, Z., and Stillman, B. (2009). The elongator complex interacts with PCNA and modulates transcriptional silencing and sensitivity to DNA damage agents. PLoS Genet. *5*, e1000684.

Lohr, D., Venkov, P., and Zlatanova, J. (1995). Transcriptional regulation in the yeast GAL gene family: a complex genetic network. FASEB J. *9*, 777–787.

Otero, G., Fellows, J., Li, Y., de Bizemont, T., Dirac, A.M., Gustafsson, C.M., Erdjument-Bromage, H., Tempst, P., and Svejstrup, J.Q. (1999). Elongator, a multisubunit component of a novel RNA polymerase II holoenzyme for transcriptional elongation. Mol. Cell *3*, 109–118.

Rahl, P.B., Chen, C.Z., and Collins, R.N. (2005). Elp1p, the yeast homolog of the FD disease syndrome protein, negatively regulates exocytosis independently of transcriptional elongation. Mol. Cell *17*, 841–853.

Rummel, R. (1976). Understanding correlation. http://www.hawaii.edu/powerkills/UC.HTM.

Santisteban, M.S., Hang, M., and Smith, M.M. (2011). Histone variant H2A.Z and RNA polymerase II transcription elongation. Mol. Cell. Biol. *31*, 1848–1860.

Schmidt, G.W., Cuny, A.P., and Rudolf, F. (2018). Preventing photomorbidity in long-term multi-color fuorescence imaging of S. cerevisiae and S. pombe. bioRxiv. https://doi.org/10.1101/180018.

Schneider, C.A., Rasband, W.S., and Eliceiri, K.W. (2012). NIH to Image to ImageJ: 25 years of image analysis. Nat. Methods *9*, 671–675.

Sood, V., and Brickner, J.H. (2017). Genetic and Epigenetic Strategies Potentiate Gal4 Activation to Enhance Fitness in Recently Diverged Yeast Species. Curr. Biol. *27*, 3591–3602.e3.

Sood, V., Cajigas, I., D'Urso, A., Light, W.H., and Brickner, J.H. (2017). Epigenetic Transcriptional Memory of *GAL* Genes Depends on Growth in Glucose and the Tup1 Transcription Factor in *Saccharomyces cerevisiae*. Genetics *206*, 1895–1907.

Stockwell, S.R., and Rifkin, S.A. (2017). A living vector field reveals constraints on galactose network induction in yeast. Mol. Syst. Biol. *13*, 908.

Stockwell, S.R., Landry, C.R., and Rifkin, S.A. (2015). The yeast galactose network as a quantitative model for cellular memory. Mol. Biosyst. *11*, 28–37.

Svejstrup, J.Q. (2007). Elongator complex: how many roles does it play? Curr. Opin. Cell Biol. *19*, 331–336.

Tong, A.H., and Boone, C. (2007). High-Throughput Strain Construction and Systematic Synthetic Lethal Screening in *Saccharomyces cerevisiae*. Method. Microbiol. *36*, 369–386, 706–707.

Tong, A.H., Evangelista, M., Parsons, A.B., Xu, H., Bader, G.D., Pagé, N., Robinson, M., Raghibizadeh, S., Hogue, C.W., Bussey, H., et al. (2001). Systematic genetic analysis with ordered arrays of yeast deletion mutants. Science *294*, 2364–2368.

Villeneuve, L.M., Reddy, M.A., and Natarajan, R. (2011). Epigenetics: deciphering its role in diabetes and its chronic complications. Clin. Exp. Pharmacol. Physiol. *38*, 451–459.

Winkler, G.S., Kristjuhan, A., Erdjument-Bromage, H., Tempst, P., and Svejstrup, J.Q. (2002). Elongator is a histone H3 and H4 acetyltransferase important for normal histone acetylation levels in vivo. Proc. Natl. Acad. Sci. USA *99*, 3517–3522.

Wittschieben, B.O., Otero, G., de Bizemont, T., Fellows, J., Erdjument-Bromage, H., Ohba, R., Li, Y., Allis, C.D., Tempst, P., and Svejstrup, J.Q. (1999). A novel histone acetyltransferase is an integral subunit of elongating RNA polymerase II holoenzyme. Mol. Cell *4*, 123–128.

Zacharioudakis, I., Gligoris, T., and Tzamarias, D. (2007). A yeast catabolic enzyme controls transcriptional memory. Curr. Biol. *17*, 2041–2046.

Zhou, B.O., and Zhou, J.Q. (2011). Recent transcription-induced histone H3 lysine 4 (H3K4) methylation inhibits gene reactivation. J. Biol. Chem. *286*, 34770–34776.

STAR★METHODS

KEY RESOURCES TABLE

REAGENT or RESOURCE	SOURCE	IDENTIFIER
Antibodies		
anti-GFP, rabbit	Thermo Fisher Scientific	Cat# A-11122; RRID:AB_221569
anti-rabbit, goat	Jackson ImmunoResearch Labs	Cat# 111-035-003; RRID:AB_2313567
anti-H3, mouse	Abcam	Cat# ab1791; RRID:AB_302613
Bacterial and Virus Strains		
XL1-Blue competent cells	Agilent	Cat# 200249
DH5α competent cells	Thermo Fisher Scientific	Cat# 18265017
Chemicals, Peptides, and Recombinant Proteins		
Turbo DNase	Thermo Fisher Scientific	Cat# AM2239
Immobilon Western HRP Substrate	Merck	Cat# WBKLS0500
Clarity ECL Western Blotting Substrates	Bio-Rad	Cat# 1705060
clonNat (Nourseothricin)	Jena Bioscience	Cat# AB-101L
G418 sulfate (Geneticin)	Calbiochem/Merck	Cat# 345810
Drop-out Mix Complete w/o Yeast Nitrogen Base	US Biological	Cat# D9515
Yeast Nitrogen Base without Amino Acids	Becton Dickinson	Cat# 291940
D-(+)-raffinose	Sigma-Aldrich	Cat# 83400
D-(+)-galactose	Sigma-Aldrich	Cat# G6404
D-(+)-glucose	Sigma-Aldrich	Cat# G8270
cycloheximide	Sigma-Aldrich	Cat# C7698
sodium butyrate	Alfa Aesar	Cat# A11079
nicotinamide	Sigma-Aldrich	Cat# N3376
micrococcal nuclease	Thermo Fisher Scientific	Cat# EN0181
formaldehyde	Sigma-Aldrich	Cat# F8775
Critical Commercial Assays		
YeaStar RNA kit	Zymo Research	Cat# R1002
ABsolute Blue qPCR SYBR green mix	Thermo Fisher Scientific	Cat# AB4162B
RevertAid First Strand cDNA Synthesis kit	Thermo Fisher Scientific	Cat# K1622
QIAquick PCR purification	QIAGEN	Cat# 28104
Experimental Models: Organisms/Strains		
Saccharomyces cerevisiae; See Tables S1 and S4 for a full list of yeast strains used in this study.	N/A	N/A
Oligonucleotides		
See Table S2 for a full list of oligonucleotides used in this study.	N/A	N/A
Recombinant DNA		
pKT355	Addgene/Kurt Thorn	RRID:Addgene_44643
pMaM4	Michael Knop lab	Khmelinskii et al., 2012
p4339	Charlie Boone lab	http://sites.utoronto.ca/boonelab/sga_technology/index.shtml
PL1603	this study	N/A
Software and Algorithms		
ImageJ 64 bit	Wayne Rasband NIH	version 1.42 Schneider et al., 2012
PhyloCell and Autotrack	Gilles Charvin	https://github.com/gcharvin Goulev et al., 2017
pyABC	Emmanuel Klinger	https://github.com/icb-dcm/pyabc Klinger et al., 2018

(*Continued on next page*)

Continued

REAGENT or RESOURCE	SOURCE	IDENTIFIER
stochastic delay model	Carsten Marr	https://github.com/ccmarr/yeast-delay
Nikon NIS Elements	MathWorks	version 4.51.c1
Visual Basic scripts	Sebastian Maerkl lab	http://128.179.34.6/twiki/bin/view/CellImaging/WebHome Dénervaud et al., 2013
MATLAB	MathWorks	versions R2009a, R2016a, and R2016b
Python	Python Software Foundation	versions 2.7 and 3.6.3
R	R Foundation for Statistical Computing	version 3.4.4

RESOURCE AVAILABILITY

Lead Contact

Further information should be directed to and will be fulfilled by the Lead Contact, Robert Schneider (robert.schneider@helmholtz-muenchen.de).

Materials Availability

The reagents generated in this study are available upon request from the Lead Contact, Robert Schneider (robert.schneider@helmholtz-muenchen.de).

Data and code availability

Data and analysis scripts for cell-tracking microfluidics are available from the authors upon request. PhyloCell and Autotrack softwares are available on Github (https://github.com/gcharvin). Code for stochastic delay model is available on Github (https://github.com/ccmarr/yeast-delay). Datasets generated from the high-throughput microfluidics screen are available upon request from Sebastian Maerkl.

EXPERIMENTAL MODEL AND SUBJECT DETAILS

Construction of the Gal1 reporter yeast strains

A precursor (RSY15) to the Gal1-GFP reporter strains RSY17 and RSY208 was constructed in parent strain Y7092 (SGA WT query strain, MATα *can1Δ*::STE2prSp_his5 *lyp1Δ his3Δ1 leu2Δ0 ura3Δ0 met15Δ0*) (Tong and Boone, 2007) as a C-terminal fusion with GFP by transformation of a PCR product containing a superfolder GFP fused to a *CLN2* PEST sequence with a kanMX cassette for selection using oligos OL2078 and OL2079 and plasmid pMaM4 (Khmelinskii et al., 2012) as a template. The selection marker in this strain was changed to natMX (conferring resistance to clonNAT/Nourseothricin) to produce RSY17 (for selection during library construction) by PCR-mediated homologous recombination of natMX amplified by oligos OL2080 and OL2079 from plasmid p4339. For cell-tracking microfluidics experiments, RSY17 was also transformed with plasmid PL1603 containing an integrating nuclear marker consisting of an NLS-fused 2mCherry to create RSY208. For the RSY19 strain where *GAL1* is replaced with GFP, and *GAL3* is tagged with mCherry, the same strategy as above was used for integrating GFP, except that instead of a C-terminal fusion, the *GAL1* ORF was fully replaced with GFP by transformation of a PCR product containing a superfolder GFP fused to a *CLN2* PEST sequence with a kanMX cassette for selection using oligos OL2306 and OL2079 and plasmid pMaM4 as a template to first create strain RSY14. The kanMX marker in RSY14 was changed to natMX to produce RSY16 by PCR-mediated homologous recombination of natMX amplified by oligos OL2080 and OL2079 from plasmid p4339. *GAL3* was then tagged with mCherry by transformation of a PCR product including mCherry with the *HIS5* selection marker using oligos OL2307 and OL2308 and plasmid pKT355 as a template.

High-throughput Gal1 reporter/mutant yeast library construction

The Gal1-GFP reporter query strain (RSY17, mat α, containing natMX for clonNat resistance) was crossed to the SGA single-deletion collection of non-essential genes (Costanzo et al., 2010) to result in a chromatin-focused library containing 567 strains. The SGA library consists of 4,309 BY4741 (MATa *his3Δ1 leu2Δ0 ura3Δ0 met15Δ0*) (Brachmann et al., 1998) single knockout strains each carrying a deletion of a non-essential gene that is replaced with the antibiotic marker kanMX, which confers resistance to G418 (Geneticin). In addition to the single-deletion strains, our SGA library contains a control strain in which the kanMX cassette has been inserted at the *LEU2* locus, specifically between chromosomal position chrIII:84678-92738. Through an automated selection process, diploid cells were sporulated, germinated and passaged as previously described (Costanzo et al., 2010), using a BM3BC colony-processing robot (S&P Robotis Inc.) to isolate haploids containing both natMX and kanMX for the reporter and

deletion cassettes, respectively. Mutants containing the *GAL1* reporter in combination with a specific gene deletion were isolated as described (Costanzo et al., 2010), with the following modifications to improve population purity (Kyriakou et al., 2016): a) strains were pinned 2 times (instead of 1) on media selecting for *can1Δ*, *lyp1Δ* and STE2prSp_his5, and b) strains were pinned 2 times (instead of 1) on media selecting for double deletions. After the final selection of haploid strains, a chromatin-focused library was created using a re-array procedure on the BM3-SC robot. Specifically, the library contained 567 yeast strains of which 535 carried deletions of known non-essential chromatin-associated factors, and also included 31 deletion strains that were randomly selected non-chromatin associated factors and 1 control strain in which kanMX was inserted at the *LEU2* locus. Selected strains were verified by junction PCR to detect the presence of corresponding kanMX and natMX cassettes and absence of WT alleles.

Reconstruction of selected candidates

For validation of their screen phenotypes, RSY208 was transformed with PCR products of kanMX to recreate 30 selected candidate deletion strains by PCR-mediated homologous recombination. Oligonucleotides are listed in Table S2.

Yeast media

Standard yeast media were used. Yeast transformations were done in YPD supplemented with antibiotics for a final concentration of 100 ug/mL clonNat (Nourseothricin, Jena Bioscience) and/or 500 ug/mL G418 Sulfate (Geneticin, Calbiochem/Merck Millipore). Microfluidics, qPCR, and western experiments were carried out in Synthetic Complete (SC) medium made with dropout mix (US Biological) and YNB + AmSO4 without amino acids (Becton Dickinson) supplemented with 1.5%–2% final concentration of raffinose (raf, Sigma-Aldrich), glucose (glu, Sigma-Aldrich), or galactose/raffinose (gal/raf, Sigma-Aldrich). For these experiments, cells were grown overnight in raf medium, then diluted in raf medium to obtain log phase cultures. Yeast were then subject to memory media change protocols including 4 hr repression in glu (r1), 1.5-3 hr induction in gal/raf (i1), followed by a second 4 hr repression in glu (r2) and a second induction in gal/raf (i2), followed by a final repression in glu (r3). Additional media for library construction are as previously described (Tong et al., 2001). Cycloheximide experiments included cycloheximide (Sigma-Aldrich) at a final concentration of 1-2 ug/mL during induction and for 30 min after the change to repression, sufficient time for Gal1 mRNAs to be degraded, ensuring that transcribed RNAs produced in i1 were not translated.

METHOD DETAILS

Plasmid construction

Plasmid pY064 was constructed by cloning in a Cln2 PEST degron sequence from pGC05D at the C terminus of a superfolder GFP in pMaM4. Plasmid pY064 was constructed by cloning in an ~1 kb upstream region of the *URA3* promoter (amplified by oligos OL2089 and OL2090 with genomic DNA from RSY17) into plasmid PL1603 containing the Nab2NLS-2mCherry nuclear marker for homology-directed integration in the Ura3 region in Y7092. Plasmids were cloned using XL1-Blue (Agilent) and DH5α (Thermo Fisher Scientific) chemically competent cells.

RT-qPCR

RNA was extracted from logarithmically growing yeast (O.D. ~0.5) using the YeaStar RNA kit (Zymo Research), and purified RNA was digested with Turbo DNase (Thermo Fisher Scientific), which was heat inactivated at 65°C for 10 min. cDNA was generated with an oligoDT primer using the RevertAid First Strand cDNA Synthesis kit (Thermo Fisher Scientific). qPCRs were performed using ABsolute Blue qPCR SYBR green mix (Thermo Fisher Scientific) and cDNA samples with Gal1-specific qPCR primers, oligos OL2091 and OL2092 in a Roche Lightcycler 96 or 480. Gal1 was quantified relative to Tcm1 as a reference gene using the ΔC_T method.

Western blot

At indicated time points, an aliquot of cells was removed from logarithmically growing cultures and proteins were extracted in Laemmli SDS buffer (Kushnirov, 2000). Samples were run on 8% polyacrylamide gels, transferred to nitrocellulose, and stained with Ponceau (0.1% Ponceau S (w/v), 5% acetic acid) to control for gel loading. Membranes were blocked with 5% BSA in 1xTBST and probed with primary antibody anti-GFP (Thermo Fisher Scientific) in a 1:1000 dilution in 1% BSA, 1xTBST. Secondary antibody anti-rabbit (Jackson ImmunoResearch Labs) was used at a dilution of 1:100,000 in 1% BSA, 1xTBST and signal visualized by Immobilon (Merck) or Clarity (Bio-Rad) ECL.

Cell-tracking microscopy setup and microfluidics devices

We used a microfluidic device designed to observe single yeast cells through several generations. The chip can accommodate 16 different yeast strains or conditions simultaneously in individual microchambers (Goulev et al., 2017). Each microchamber has 8 microchannels where yeast can be captured, as well as 2 lines for cell injection and 2 major lines for the rapid exchange of media. Phase contrast and fluorescence images of live cells were recorded every 3 min via automated time-lapse microscopy using an inverted microscope (AxioObserver or Nikon Eclipse Ti-E) with epifluorescence capabilities and a temperature-controlled

stage (custom-built, IGBMC). For candidate maintenance/inheritance analyses, inductions were fixed to 3 hr for all strains, long enough to sufficiently induce Gal1 in all strains and observe differences to the WT, yet short enough for Gal1-GFP to degrade during the repressions, which were fixed to 4 hr.

Cell-tracking data processing and analysis

We used custom-made PhyloCell and Autotrack softwares (available on Github https://github.com/gcharvin) written in MATLAB (MathWorks) for image segmentation, cell-tracking, fluorescence measurements, and lineage analysis (Goulev et al., 2017).

Gal1 intensity

Gal1-GFP fluorescence was measured and normalized to cell area. Background autofluorescence was calculated by averaging the fluorescence in cell contours over an interval at the beginning of i1 and subtracted from intensity measurements when necessary. Intensities are reported for the end of the induction phase unless otherwise stated.

Gal1 delay

Gal1 delay represents the time difference from the start of galactose exposure until detectable fluorescence. Delay was defined by a positive derivative of Gal1 intensity over 3 frames on smoothed intensity traces (over 4 frames) in order to minimize the effect of spurious intensity fluctuations. Non-inducers with no computed delay were not included in figures displaying delays, including Figures 1D middle and right, 2D, 4A–4C, 4E, 4F, and S4C bottom.

Mother and daughter definitions

Nuclear division markers (NLS-tagged mCherry) were used to automatically define relationships between mother cells (Ms) and their specific daughters (Ds) and record their birthtime in PhyloCell. Mothers are defined as cells born before i1 and therefore present throughout both inductions. Calculations with daughter cells were restricted to cells born during r2 (born after i1 and before i2), though mothers could give rise to daughters at other times (not included in our analyses).

Density estimates for delays

Density estimates used a Gaussian kernel with a bandwidth given by Scott's rule as $1/n^5$ where n is the number of data points.

Partial correlations (PCs)

PCs (Rummel, 1976) were calculated to measure the degree of association between two cells, while removing the effect of galactose induction that would result in extremely high correlations even among unrelated cells. To subtract this effect, average Gal1 expression in the population was calculated over time and used as the controlling variable. PCs for Gal1 expression over 1 hour of induction were calculated.

Expression rate

Expression rate was approximated by the slope of a line passing through the single-cell expression curve at the time of detected delay and at maximal expression.

Relative difference (RD) of delay

RD was defined as the absolute value of two delays divided by the sum of the delays. RDs were calculated for the time delay until Gal1 expression for each mother to itself in i1 versus i2 or for a pair of mother and daughter cells in i2. To ensure that the effects were specific to mother-daughter pairs and not a general feature of the mutant strain, RDs were also calculated for randomized mothers and daughters using equivalent sample sizes as the related cells; in these randomized pairs, no difference was observed between the strains (data not shown).

Posterior distribution functions

Using Bayesian Statistics, a posterior distribution $P(p|k,N)$ was calculated where p is the probability that the mother expresses before its daughter given the data (k,N) :

$$P(p|k,N) = \frac{L(k|p,N)\cdot\pi(p)}{\int L(k|p,N)\cdot\pi(p)dp}$$

Where L is a binomial likelihood, and $\pi(p)$ is a *Beta* $(1,1)$ flat prior distribution. In this case, we were interested in the probability that mothers express earlier more than 50% of the time. Thus we calculated the posterior probability that p was larger than 0.5 by integrating $P(p|k,N)$ on the interval [0.5,1]. A probability outcome of 0.5 would then indicate that neither mothers nor daughters express earlier than the other group.

Growth rates

Doubling times were calculated according to Schmidt et al. (2018). Briefly, total cell area (A) in images at 2 time points (t_1 and t_2) was used to determine growth rate with the following equation:

$$doubling\ time = \frac{(t_2 - t_1)\cdot log(2)}{\log(A_{t2}) - \log(A_{t1})}$$

High-throughput microfluidics and microscopy setup

For library screening, we used a "microchemostat" microfluidic platform containing an array of 1,152 microchambers each of which can be filled with a different yeast strain, with an integrated valve system to allow for a single flow of medium through the whole array as well as automated media changes (Dénervaud et al., 2013). Images were captured at 60x magnification with 10-minute

resolution for each strain, and then were segmented and analyzed with a custom platform. Each experiment contained 2 technical replicates for each strain spotted in different locations on the chip to avoid experimental biases, with 3 biological replicates of the screen.

Screen data processing and analysis

Data measurements

For each strain the mean, median, and standard deviation of Gal1 intensity was monitored over time. All values were collected using the standard background subtraction method and are in arbitrary units. In addition, for each time point the percentage of cells that are expressing Gal1 was calculated using an intensity threshold of 150 a.u. When necessary, linear regression was used to adjust for any gradient in nutrients due to diffusion rates through each chemostat.

Quality control

The whole microfluidics device was imaged during overnight growth in raf at 4x magnification. Microchambers that were not completely filled with cells by the start of the memory experiment were excluded from analysis. For quality control within the microfluidics device, any row of cells with markedly different Gal1 expression or growth rate was eliminated from analysis.

Intensity and induction timing analysis of screen data

For Gal1 expression level, we estimated the intensity of GFP fluorescence using a weighted linear fit. The weight w_{TP} was necessary to avoid fitting out-of-focus images and relied on the number of properly defined cells NbC_{TP} from the segmentation at the respective time point TP

$$w_{TP} = \frac{NbC_{TP}^2}{50^2 + NbC_{TP}^2}$$

The fit used the data acquired between 30 min before and after the estimated time point to include 3 frames for each microchamber. To estimate Gal1 induction timing, we fit a smoothed cubic spline to time points after the start of the respective inductions. We used an intensity threshold to identify induced cells in i1 and defined a minimum percentage of induced cells i_0, using the minimum percentage of expressing cells 1 hr prior to i1 (~0%), or the minimum percentage of expressing cells ± 20 min from the start of i2. If necessary for some strains where not all cells returned to background levels during r2 prior to the start of i2, we additionally used a percentage threshold. The threshold $delT_1$ for delay time was composed of the fixed induced percentage threshold parameter $delT_0$ and the estimated value of induced cell percentage during the beginning of induction a_0

$$delT_1 = i_0 + (1 - i_0) \cdot delT_0$$

We chose an induced cell threshold $delT_0$ of 50% as this represents the median of cells expressing Gal1 and also because the medium shape of the induced cell percentage over time can be approximated by a logistic function, which is the steepest for 50%, making it the threshold with the smallest theoretical estimation error.

Data condensation of screen biological replicates

To allow the merged representation of all 3 experimental repeats, we applied locally weighted scatterplot smoothing (LOESS). We used the mean of repeats from the 3 experiments to compute a local regression curve for each of the 4 data points (intensity and delay during i1 and i2) in each experiment. These curves were then used to standardize all individual microchambers toward an average experiment.

Outlier detection (strains of interest)

Our complex dataset justified testing a number of methods for outlier identification. We identified outliers in the 2D distributions of our unmerged and condensed datasets according to intensity and delay values by using a cutoff-based approach to detect strains that are repeatedly different from the norm. First, outlier cutoffs were made for i1 by combining a percentage-based cutoff with an interquartile range approach. For this, the percentage was set at the 2% and 98% quartile and r for the interquartile range was set as 1, ~2% for a normal distribution. For i2, the data points were first sorted after their i1 values. We then used a moving window of 11 data points combined with the interquartile range to obtain moving thresholds for upper and lower outliers using cubic smoothing splines to get smooth curves for these values.

Candidate validation

WT reference response curve

To characterize the memory exhibited by the WT as a reference, we measured the peak Gal1 intensities in i1 and i2 for 5 induction lengths ranging from 96 min to 180 min (equal for i1 and i2 within the same experiment), in 13 time-lapse microfluidics experiments with a total of 121 microchamber positions. We characterized the WT memory by determining a response curve which gives the average i2 induction for a given i1 induction, $I2_{ref}(I1)$, as follows. First we performed a kernel density estimate of the conditional probability $p(I2|I1)$ to observe an average peak i2 induction level $I2$ after average peak i1 level $I1$. We then interpolated its quantiles at 0.5, 0.32 and 0.68 using a smoothing spline, which produced the mean response $I2_{ref}(I1)$ (solid line in Figure S4A) with lower and upper boundary lines (dashed lines in Figure S4A).

Signed distance to the WT response curve

30 mutant candidates recreated by PCR-mediated homologous recombination were also induced for induction lengths from 96 to 180 min in 21 microfluidics experiments, covering 106 microchambers with each strain represented in at least 8 microchambers. Candidates were measured for their deviation from the WT response at equivalent induction lengths by calculating a deviation measure for each microchamber containing the strain of interest, given as a Z-score, that is, normalized by the corresponding range of WT variability, as follows:

$$d(I2) = \frac{I2 - I2_{\mathrm{ref}}(I1)}{\left| I2_{\mathrm{sigma}}(I1) - I2_{\mathrm{ref}}(I1) \right|},$$

Here, $I2_{\mathrm{sigma}}(I1)$ is the interpolated quantile at 0.32 for $I2 < I2_{\mathrm{ref}}(I1)$ and at 0.68 for $I2 > I2_{\mathrm{ref}}(I1)$, respectively. Lines of equal deviation at $d = \pm 1, \pm 3, \pm 5$ are shown in Figure 3D.

To assess whether mutant data fall within or outside the WT range of responses, we compared the measured deviations d of each mutant candidate with those of the WT, using a two-sample Anderson-Darling (AD) test. Candidates were then ranked according to statistical significance based on AD scores.

Mathematical Modeling

Stochastic delay model

Gal1 promoter activation was modeled as a sequential stepwise process with two parameters (Figure 5B): the number of activation steps n and the rate of each step α, which we assume to be the same for each step for simplicity. The corresponding delay time (i.e., the time needed to reach the active state A from the inactive state I, Figure 5B) is Erlang-distributed with mean n/α. This allows us to quantitatively fit the delay distributions of cells in i2 (Figure 4B) with a simple Erlang distribution, and likewise the relative difference of mother and daughter cells in i2 (Figure 4E) with the relative difference of two Erlang-distributed random variables. For fitting, we use the likelihood free pyABC package (Klinger et al., 2018) which allows us to consider both delay and relative difference. Apart from the model, we specify the prior distribution for $n \in$ [1,20] and $\alpha \in$ [0.1,15] 1/min and the distance function. To fit both delay and relative difference, which are on different scales (Figures 4B and 4E), we normalize the mean and the variance of the delay with the mean and variance observed in the data, respectively, and divide the mean and variance of the delay distribution by the variance of the data and the square root of the number of data points, respectively. The posterior estimates for the parameters show similar rates, but different activation steps. We simulate delay and relative difference with 10 steps for WT and 6 steps for the *elp6Δ* mutant and find that a reduced number of activation steps can explain both reduced delay and at the same time, a larger mother-daughter relative difference (Figure 5D). For implementation details, the Jupyter notebook is available on Github (https://github.com/ccmarr/yeast-delay).

Chromatin immunoprecipitation (ChIP)

ChIP sample collection

Strains were subjected to memory time courses involving media changes for cycling repressions and inductions and were maintained at OD ~0.5 throughout. For each ChIP time point collected, samples were also collected for RT-qPCR to ensure Gal1 was induced and showed memory. For each ChIP time point, 9x10^8 cells were crosslinked at room temperature for 30 min with 1% formaldehyde (enough for ~10 IPs). All strains were crosslinked with the same number of cells and volume at each time point; when necessary, medium was added to make all cell densities equivalent. Cells were washed 1x with 10 mL cold PBS, 1x with 10 mL cold PBS+histone deacetylase inhibitors (50 mM sodium butyrate (Alfa Aesar) and 5 mM nicotinamide (Sigma-Aldrich), and frozen pellets were stored at −80°C.

Chromatin preparation and IPs

Cell pellets were lysed using zirconia beads on a BeadBeater (Biospec) in SDS buffer (50 mM Tris-HCl pH 8.0, 10 mM EDTA, 1% SDS, protease inhibitors, 5 mM nicotinamide, 50 mM sodium butyrate). Supernatants were sonicated (Qsonica) to an average of ~200 bp. Chromatin was diluted with IP buffer (16.7 mM Tris-HCl pH 8.0, 1.2 mM EDTA, 1.1% Triton X-100, 0.01% SDS, 167 mM NaCl, protease inhibitors, 5 mM nicotinamide, 50 mM sodium butyrate) and then precleared with preblocked beads and 1/10 was used for each IP. H3 antibody (Abcam ab1791) was incubated with chromatin and IPed with a mixture of IgG and IgA beads. IPs were washed 1x with TSE-150 wash buffer (20 mM Tris-HCl pH 8.0, 2 mM EDTA, 150 mM NaCl, 1% Triton X-100, 0.1% SDS), 1x with TSE-500 wash buffer (20 mM Tris-HCl pH 8.0, 2 mM EDTA, 150 mM NaCl, 1% Triton X-100, 0.1% SDS), 1x with LiCl wash buffer (10 mM Tris-HCl pH 8.0, 1 mM EDTA, 1% sodium deoxycholate, 1% NP-40, 250 mM lithium chloride), and a final wash in TE buffer (10 mM Tris-HCl pH 8.0, 1 mM EDTA) before elution with 100 mM sodium bicarbonate and 1% SDS. Samples were reverse crosslinked, treated with RNase A and Proteinase K, then purified (QIAquick PCR purification) and used for qPCR.

ChIP-qPCR

qPCRs were performed using ABsolute Blue qPCR SYBR green mix (Thermo Fisher Scientific) and ChIP samples with *GAL1* promoter-specific qPCR primers, oligos OL2243 and OL2244, in a Roche Lightcycler 96 or 480. H3 was quantified at the *GAL1* promoter relative to input. H3 ChIPs in mutant strains were normalized to WT within each time point.

Nuclease sensitivity

Nuclease sensitivity sample collection

Samples were collected and digested with micrococcal nuclease (MNase) as previously with minor changes (Bryant et al., 2008). Briefly, WT and *elp6Δ* were subjected to memory time courses as for ChIP. For each sample, 100 mL of OD 0.5 cells were crosslinked at room temperature for 5 min with a final concentration of 0.5% formaldehyde (Sigma-Aldrich). Formaldehyde was quenched with final 0.125 M glycine and washed 1x with 10 mL cold PBS and frozen pellets were stored at −80°C.

Chromatin preparation and nuclease digestion

Cell pellets were lysed using zirconia beads on the BeadBeater with FA lysis buffer without EDTA (50 mM HEPES-KOH (pH 7.5), 140 mM NaCl, 1% Triton X-100, 0.1% sodium deoxycholate). For each digestion, 26 uL of supernatant was diluted with 120 uL FA lysis buffer without EDTA and then 10 uL of an MNase (Thermo Fisher Scientific) solution ranging from 0.125 – 4 units was added with an undigested sample for reference. Digestions were started by adding 5.6 uL of 2 mM $CaCl_2$ and incubated at 37 deg for 1.5 hours. Reactions were quenched with the addition of 8.8 uL 0.5 M EDTA, and SDS and NaCl were added to a final concentration of 1% and 200 mM, respectively. Samples were reverse crosslinked and treated with Proteinase K by incubating at 42 deg for 1 hour followed by 65 deg for at least 4 hours, then purified (QIAquick PCR purification) and used for qPCR.

MNase-qPCR

qPCRs were performed using ABsolute Blue qPCR SYBR green mix and nuclease sensitivity samples with *GAL1* promoter-specific qPCR primers, oligos OL2282 and OL2283, in a Roche Lightcycler 96 or 480. Amplicons in each digested sample are relative to undigested sample *GAL1* using the ΔC_T method. Shown is the ratio of WT to *elp6Δ* (where templates were digested with the same MNase concentration within one experiment).

QUANTIFICATION AND STATISTICAL ANALYSIS

We used t test, Kolmogorov-Smirnov (KS), Anderson-Darling (AD), and Mann-Whitney *U* (MW) tests to assess statistical significance. For t test, we used Bonferroni correction for multiple testing. For KS we used two-sided tests, and for Anderson-Darling we used two-sample tests. For MW, we used two-sided non-parametric tests with Bonferroni correction for multiple testing. Box-plot elements are as follows: center line, median; diamond, mean; box limits, upper and lower quartiles; whiskers, 1.5x interquartile range; points, outliers. In figures, *n* denotes the number of single cells included in each analysis. *P*-value significances are denoted in figures by ns (not significant) > 0.05, * ≤ 0.05, ** ≤ 0.01, *** ≤ 0.001 **** ≤ 0.0001, with exact *P*-values and details of the statistical tests in Table S3.